Journal of Molecular Liquids 393 (2024) 123550

Contents lists available at ScienceDirect

Journal of Molecular Liquids

journal homepage: www.elsevier.com/locate/molliq

Disclosing the nature of the collective THz dynamics in hydrogen bonded liquids

M. Zanatta [a,*], A. Orecchini [b,c], F. Sacchetti [b,c], C. Petrillo [b]

[a] Dipartimento di Fisica, Università di Trento, via Sommarive 14, I-38123, Trento, Italy
[b] Dipartimento di Fisica e Geologia, Università di Perugia, Via A. Pascoli, I-06123 Perugia, Italy
[c] IOM-CNR, c/o Dipartimento di Fisica e Geologia, Università di Perugia, Via A. Pascoli, I-06123 Perugia, Italy

ARTICLE INFO

Keywords:
Molecular liquids
Water
Collective excitations
Inelastic neutron scattering

ABSTRACT

The behavior of liquids has always been a subject of strong interest and still presents many challenging issues. A paradigmatic example is the understanding of their atomic-scale collective dynamics. Experimentally accessible to inelastic neutron and X-ray scattering, this regime has recently disclosed an unexpectedly rich scenario made up of more than one collective excitation. However, experiments lack a fundamental piece of information since they cannot distinguish the longitudinal or transverse nature of the detected modes. Here we present an inelastic neutron scattering study of the atomic dynamics of water and sulfuric acid, two prototypes of hydrogen bonded liquids. We propose a novel method that allows the experimental determination of the nature of the observed modes, without resorting to any indirect information. The dynamic structure factors show a complex collective dynamics, with two propagating excitations that we describe in the framework of an interacting-modes model. The first high-energy excitation is usually assumed to be the prolongation of the longitudinal acoustic mode and is characterized by a strong fast sound, which in turn we ascribe to the interaction with the second low-energy mode. Our approach confirms the main longitudinal nature of the first mode and unambiguously identifies the transverse nature of the second one. Finally, the lifetime of the modes suggests a common origin for the second mode, possibly related to the presence of the hydrogen bond network.

1. Introduction

Macroscopically, a liquid at equilibrium is homogeneous and isotropic. Its dynamics is well described by classical hydrodynamics, where only longitudinal waves can propagate. Microscopically, the liquid phase is characterized by large atomic displacements that coexist with strong interatomic interactions. In such a scenario the standard theoretical tools used for solids and gases have limited effectiveness [1]. Indeed, at the nanometer and picosecond length- and time-scale, i.e. in the THz frequency regime, continuous translational and rotational symmetries break down, and the atomic dynamics discloses a surprisingly rich scenario. Ranging from water [2–5] to liquid metals [6,7], a large number of systems shows more than one excitation with well-defined dispersion curves up to relatively high exchanged wavevector Q. To completely understand the THz dynamics of liquids, we thus have to correctly identify the nature of these observed modes. In principle, inelastic neutron scattering (INS) and inelastic X-ray scattering (IXS) can detect only the longitudinal component of density fluctuations. Consequently, predominantly transverse modes are visible only through their longitudinal projections and must vanish in the hydrodynamic regime. Here, we carry out coherent INS experiments to measure the dispersion curves of collective modes in liquids. Following a crystal-like approach, we work out the single-mode density of states (DOS), that we finally compare to the density of states $g(\omega)$ measured by incoherent INS. Such a comparison provides a quantitative and experimental assessment of the nature of the observed modes. We show the validity of this method by analyzing the THz dynamics of two hydrogen-bonded model liquids, i.e. water and sulfuric acid.

Widely present in nature, hydrogen-bonded liquids represent a particularly interesting class of systems. Their distinctive feature is the presence of an extended but fluctuating hydrogen bond network that plays a key role in many chemical and biological processes [8]. Within this class, water (H_2O) definitely attracted much interest for its *anomalous* behavior and its prominent role in nature and life [9]. Its THz

* Corresponding author.
E-mail address: marco.zanatta@unitn.it (M. Zanatta).

https://doi.org/10.1016/j.molliq.2023.123550
Received 16 June 2023; Received in revised form 6 November 2023; Accepted 8 November 2023
Available online 14 November 2023

dynamics is characterized by a dispersive mode accompanied by a second, low-lying, non-propagating excitation [2–5]. The behavior of the first mode suggests its identification as the longitudinal acoustic one, whereas the nature of the low-lying excitation is less defined, although it is often ascribed to the local structure of the H-bond network [10,11]. The longitudinal mode has a high-frequency propagation velocity c_∞ that is about a factor two greater than c_0, the low-frequency one [12,13,3]. This phenomenon is named *fast sound* and was first observed in molecular dynamics simulations of water [14]. The anomalous slow-to-fast sound transition has been alternatively ascribed to structural relaxations [15] or to an interaction between the two modes [4]. These two alternative scenarios use a different formal approach but are both based on the interaction of the acoustic mode within a complex environment. A similar, and partially alternative, view was proposed by Ishikawa and Baron [16] who discussed the two observed modes within a hydrodynamic model as the interaction of a longitudinal acoustic mode and a diffusion-like dynamics. This view can be seen as a variant of the relaxation model but the experimental data available nowadays are still not accurate enough for a real comparison of these models also because there is not substantial difference when used in comparison to the data. Interestingly, the transition from c_0 to c_∞ was observed also in disordered systems like glasses, where both relaxations and mode interactions are present. However, water and hydrogen-bonded systems remain peculiar, with a ratio $c_\infty/c_0 \geq 2$. Indeed, this was observed in systems with different H-bond networks and strength: HF [17] and NH_3 [18,19], protein hydration water [20], dry proteins [21], DNA [22], deuterated bacteria [23], and even human cell chromatin [24]. Another example of hydrogen-bonded liquid is sulfuric acid H_2SO_4. Well known for its role in industrial applications, sulphuric acid is also common in Nature, both on Earth and in extra-terrestrial space [25]. It is present on the icy satellites of the outer Solar System [26], in the atmosphere of Venus [27] and as a contaminant of Earth atmosphere [28]. Although chemically different, at room temperature and pressure sulfuric acid shows a structure similar to water, in both the solid and liquid phase, with shorter and stronger hydrogen bonds [29–31]. Both systems have an almost tetrahedral local arrangement, so that each molecule is bonded to other four molecules forming, on the average, a tetrahedral. The molecular number density n_m of H_2SO_4 (0.0111 molecules/Å^3) is three times lower than H_2O (0.0330 molecules/Å^3). This is due to the size of the SO_4 units compared to the oxygen atom. Notably, in ice a single H-atom randomly occupies two possible sites along the O-O bond, according to the Pauling rules, whereas in solid sulfuric acid, a single H-atom occupies a defined position [29].

2. Materials and methods

Our approach is based on the comparison between collective modes, determined from the dynamic structure factor $S(Q,\omega)$, and the $g(\omega)$. These quantities can be obtained by INS: the first on a coherent sample, the second measuring the self dynamic structure factor $S_s(Q,\omega)$ on a incoherent sample [32]. In the case of water and sulfuric acid, coherent/incoherent samples can be easily prepared by exploiting H/D isotopic substitution.

Pure water was thus measured as both coherent D_2O and incoherent H_2O. Sulfuric acid, instead, was measured in the form a slightly hydrated solution (98 wt%) to ensure good chemical stability, for both for the coherent D_2SO_4 and the incoherent H_2SO_4.

For D_2O and D_2SO_4, the ratio between the coherent to incoherent cross sections $\sigma_{coh}/\sigma_{inc}$ are 3.8 and 7.1, respectively. The single scattering intensity $I(Q,\omega)$ can be thus safely assumed proportional to the $S(Q,\omega)$. The dynamic structure factor of D_2O was measured on IN1 as described in Ref. [4]. The $S(Q,\omega)$ of D_2SO_4 was measured at 293 K on the three-axis spectrometer IN1 at the Institut Laue-Langevin (ILL, Grenoble, France). The sample was loaded in a flat molybdenum cell ($80 \times 35 \times 10$ mm^3, 0.5 mm-thick windows). Inelastic scans were performed at fixed final wave vector $k_f = 6.213$ Å^{-1} with a Cu(400) analyzer, while the incident wave vector k_i was varied by the low d-spacing Cu(331) monochromator. Very tight collimations (25', 20', 20' and 20') were applied from reactor to detector. Data were collected at eight Q-values: 0.15, 0.2, 0.25, 0.3, 0.35, 0.4, 0.5 and 0.7 Å^{-1}. The elastic energy resolution, measured on a vanadium slab of the sample size, was Gaussian-shaped with 1.62 ± 0.03 meV full width at half maximum (FWHM). The background was also measured and data were carefully reduced according to the procedure described in Ref. [4]. Due to the low molecular density ($n_m = 0.0111$ Å^{-3}), self-absorption and multiple scattering effects were small despite the thick sample and were corrected according to Ref. [33].

The density of states of H_2O and H_2SO_4 were measured at the time-of-flight spectrometer IN5 (ILL, Grenoble, France) with a fixed incident energy of 1.132 meV and an elastic energy resolution of about 26 μeV FWHM, as obtained from a vanadium sample measurement. The sample was contained in a 0.5 mm-thick hollow quartz cylinder that ensures high transmission and reduced multiple scattering. Data were analyzed assuming a negligible coherent contributions, given that $\sigma_{coh}/\sigma_{inc}$ is 0.05 and 0.13 for H_2O and H_2SO_4, respectively. Experimental background and multiple scattering were subtracted using the same procedure of the coherent scattering experiment, taking into account also the mixed multiple scattering processes between of cell and sample.

3. Results and discussion

The single scattering intensity $I(Q,\omega)$ measured for D_2O and D_2SO_4 is shown in Fig. 1 at some typical Q values. Spectra are characterized by a quasielastic line with inelastic side structures related to the collective dynamics of the sample. The quasielastic line of D_2SO_4 is resolution limited whereas D_2O shows a broadening. Considering the low-frequency sound velocity, $c_0 = 1320$ m/s for D_2O and $c_0 = 1257$ m/s for D_2SO_4, and a linear dispersion, the black arrows mark the expected positions of the collective excitations. The obtained values are not consistent with the measured inelastic features that extend up to much higher energies and clearly show the presence of fast sound in both samples.

The measured intensity $I(Q,\omega)$ is proportional to the convolution of the experimental resolution $R(Q,\omega)$ with the dynamic structure factor $S(Q,\omega) = S_{qes}(Q,\omega) + S_{ins}(Q,\omega)$, where the first term describes the quasielastic contribution and the second one accounts for the inelastic collective features. As already mentioned, the experimental $S(Q,\omega)$ is sensitive only to longitudinal density fluctuations. Since modes with the same symmetry interact with each other, the most general treatment of a system with many modes has to include their coupling to reproduce the correct inelastic shape. A general description of the interacting-modes model is found in [7] for the case of liquid metals. Early successful applications of this approach include vitreous $SiSe_2$ [34], molten zinc [6] and liquid GeTe [35]. The model provides a good description of experimental data and anticrossing of dispersion relations [37,36]. $S_{ins}(Q,\omega)$ is modeled assuming a system of only two interacting oscillators with bare energies $\hbar\omega_j$ ($j = 1,2$). Starting from the Hamiltonian of a system with interacting modes [6,7,34], $S_{ins}(Q,\omega)$ turns out to be:

$$S_{ins}(Q,\omega) = \sum_{jj'} \mathcal{F}_{jj'}(Q)\, S_{jj'}(Q,\omega), \tag{1}$$

where $\mathcal{F}_{jj'}(Q)$ is a proper structure factor and $S_{jj'}(Q,\omega)$ is the mode-mode dynamic structure factor. Assuming $\mathcal{F}_{jj'}(Q) \simeq A_j(Q)\delta_{jj'}$ and the presence of only two interacting modes, we can write:

$$S_{jj}(Q,\omega) = -\frac{n(\omega,T)+1}{\pi}\,\Im\left[\frac{\chi_j}{1-\chi_1\chi_2|U(Q)|^2}\right], \tag{2}$$

where $\chi_j \equiv \chi_j(Q,\omega) = \left\{\omega^2 - \omega_j^2(Q) - \Sigma_j(Q,\omega)\right\}^{-1}$ is the single-mode Green's function and $n(\omega,T)$ is the Bose population factor. The jth mode is characterized by the mode energy $\hbar\omega_j(Q)$ and the self-energy $\Sigma_j(Q,\omega)$, describing the interaction with the environment. This produces the large broadening of the mode response, characteristic of all

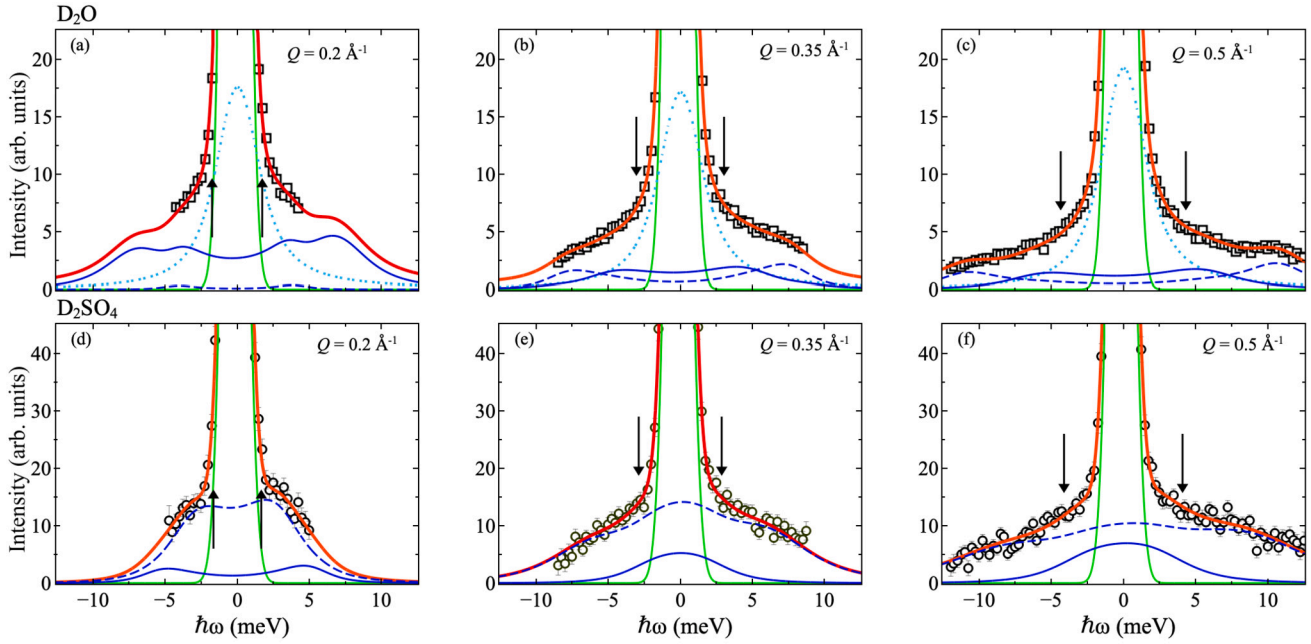

Fig. 1. Experimental data for D_2O (first row, open black squares) and D_2SO_4 (second row, open black circles) at three Q values: (a,d) 0.2 Å^{-1}, (b,e) 0.35Å^{-1}, and (c,f) 0.5 Å^{-1}. The thick red line is the best fit to the data using the interacting-modes model of Eq. (3). The solid green line shows the experimental resolution. The blue lines represent the two inelastic components $j = 1$ (solid line) and $j = 2$ (dashed line). The dotted line in D_2O is the quasielastic Lorentian contribution. The black arrows mark the expected positions of the collective modes, assuming a linear dispersion with sound velocity $c_0 = 1320$ m/s for D_2O and $c_0 = 1257$ m/s for D_2SO_4.

disordered systems. The simplest approximation having the correct ω dependence, as expected from time causality, is $\Sigma_j(Q,\omega) \simeq i\omega\Gamma_j(Q)$, where $\Gamma_j(Q)$ is the Q-dependent damping coefficient. The real part of $\Sigma_j(Q,\omega)$ is not present in this approximation. Finally, the coupling $U(Q)$ is described by a simple function including an exponential decay function $U(Q) = \beta Q \exp[-\alpha Q]$, is such that the existence of an acoustic mode is guaranteed.

Considering the experimental resolution, the quasielastic component is well approximated by a δ-function for D_2SO_4 whereas a further Lorentzian broadening term is necessary for D_2O. The $S(Q,\omega)$ can be finally written as:

$$S(Q,\omega) = S_{qes}(Q,\omega) + \sum_{j=1}^{2} A_j S_{jj}(Q,\omega), \tag{3}$$

where $A_j(Q)$ are the amplitudes of the inelastic components. It is worth noting that, when $U(Q) = 0$, $S(Q,\omega)$ is simply the sum of two damped harmonic oscillators plus the quasi-elastic contribution. However, the interaction between modes can easily explain the slow to fast sound transition. Indeed, when $Q \to 0$, neglecting the damping which is expected to decrease at low Q, we have $c_0^2 \simeq c_\infty^2 - \beta^2/[\hbar\omega_2(0)]^2$, where $j = 2$ refers to the non dispersive mode [4]. This provides a further constraint for β because c_0 is known. The above model has also some connection with the gapped collective mode description recently proposed for liquid Ga [38].

The model of Eq. (3) is rather complex and the fitting parameters as well as their stability have to be carefully considered. In particular, since the available kinematic range is strongly Q-dependent, different approaches have to be used to constraint the fit. For $Q > 0.35$ Å^{-1} all the parameters were free. The interaction parameters α and β are Q-independent and they were defined by repeating all the fit procedure and taking into account the fast sound transition $c_0 \to c_\infty$ to determine β. In this range, a reduced χ^2 ranging between 0.92 and 1.11 was found. In the range 0.2 Å$^{-1} < Q < 0.4$ Å^{-1} Γ_1 was fixed according to a linear trend extrapolated from the higher momentum data. In the range below 0.25 Å^{-1} also a fixed $\omega_1(Q) = c_\infty Q$ was employed. The so obtained low-Q fits were also stable and coherent with the results of the full fit performed in the high-Q interval.

Fig. 1 shows the good agreement between the experimental data (black symbols) and the fit with Eq. (3) (red line). The individual inelastic components (blue lines) are also plotted. The interaction mixes up the two inelastic components so that both unperturbed modes contribute to the shape of each $S_{jj}(Q,\omega)$. This is evident in the low-Q region where $S_{11}(Q,\omega)$ shows a mild double peak structure in the case of D_2O. Indeed, the interaction results in oscillator force transfer from one mode to the other, thus making visible the effect of an *almost invisible* transverse mode as a *signature* present on the *always visible* longitudinal mode, see Fig. 1. However, $S(Q,\omega)$ is sensitive only to longitudinal density fluctuations, so the relative intensity of the two components suggests a predominantly longitudinal character for $j = 1$ and a transverse nature for $j = 2$.

Figs. 2(a) and (d) show the dispersion relations of the two *bare* energies $\hbar\omega_1(Q)$ and $\hbar\omega_2(Q)$, as obtained from the fitting procedure. The high-frequency mode ($j = 1$) shows a linear dispersion and can be identified as the high-frequency prolongation of the longitudinal acoustic mode. The measured velocities are $c_\infty = 3380 \pm 50$ m/s and $c_\infty = 3360 \pm 50$ m/s, for D_2O and D_2SO_4 respectively. The c_∞/c_0 ratio turns out to be greater than 2, namely 2.73 ± 0.04 for D_2O and 2.67 ± 0.06 for D_2SO_4. It is worth noting that the c_∞/c_0 ratio in water is even greater than that obtained in the previous analysis done with two independent DHO's. Conversely, the low-lying mode ($j = 2$) shows a mild Q dependence with an average energy $\langle\hbar\omega_2\rangle = 7.0 \pm 0.3$ meV in D_2O and $\langle\hbar\omega_2\rangle = 4.7 \pm 0.8$ meV in D_2SO_4.

The mode damping factors Γ_j are plotted in Figs. 2(b) and (e). The two modes show an almost linear trend and Γ_2 has similar values both in water and in sulphuric acid. Conversely, the $j = 1$ mode shows qualitative and quantitative differences as this collective mode propagates much better than in water. In particular, Γ_1 in D_2O is almost twice smaller than in D_2SO_4. In addition, water seems to show some departure from linearity. Figs. 2(c) and (f) show the ratio Γ_j/ω_j. In D_2SO_4, the ratio Γ_1/ω_1 is almost constant with a value about 1.2, a trend similar also to that of liquid metals [39,40]. On the other hand, several

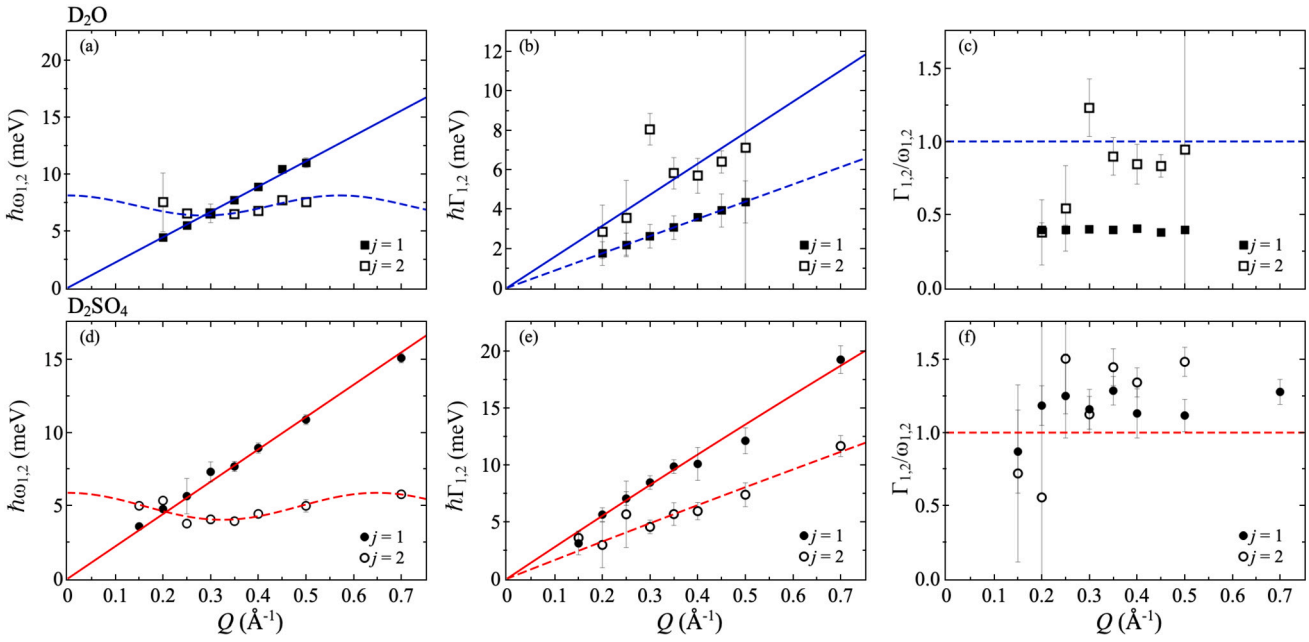

Fig. 2. Dispersion curves of the bare energies $\hbar\omega_1(Q)$ (black solid symbols) and $\hbar\omega_2(Q)$ (black open symbols) of the modes in (a) for D_2O (squares) and (d) for D_2SO_4 (circles). The solid line is the linear fit of the high-frequency longitudinal mode and provides a fast sound velocity $c_\infty = 3380 \pm 50$ m/s in D_2O $c_\infty = 3360 \pm 50$ m/s in D_2SO_4. The dashed line highlights the Q evolution of $\hbar\omega_2$. Damping parameters $\hbar\Gamma_1$ (black solid symbol) and $\hbar\Gamma_2$ (black open symbols) of the modes in (b) for D_2O (squares) and (e) for D_2SO_4 (circles). The solid and dashed lines are the linear fits of their Q evolution.

glasses [41,43,42] and biological systems [20,22,21] display a linear trend of Γ_1/ω_1, due to a rapidly increasing parabolic trend of Γ_1.

The analysis of the $S(Q,\omega)$ with Eq. (3) does not allow the identification of the specific character, either longitudinal or transverse, of the two modes. Obviously, in order to be detected, a longitudinal component must be present in both modes. However, a more quantitative analysis can be obtained by comparing the density of states derived from the $S_j(Q,\omega)$ to the experimental $g(\omega)$.

To determine the experimental density of states, measurements were carried out on incoherent H_2O and H_2SO_4 samples. The experimental details and the data reduction procedure are detailed in Sec. 2. Once obtained the $S_s(Q,\omega)$, the $g(\omega)$ on absolute scale is obtained by the $Q \to 0$ extrapolation procedure described in Ref [7].

The resulting hydrogen-projected densities of states are shown in Fig. 3 (open black symbols). We now have to connect the information obtained from $S(Q,\omega)$, i.e. the longitudinal density fluctuations, with that contained in the $g(\omega)$, i.e. the whole density of states including also transverse modes as deduced from the single-atom dynamics [32]. To do so, we can calculate the longitudinal component of the density of states of each mode:

$$g_j(\omega) = \frac{1}{K_g} n_m \int_0^{Q_M} A_j \tilde{S}_{jj}(Q,\omega) dQ, \tag{4}$$

where $\tilde{S}_j(Q,\omega)$ is the dynamic structure factor of the j-th mode obtained from the fit to Eq. (3) and properly normalized to get $\int_0^\infty \tilde{S}_j(Q,\omega)d\omega = 1$. The integration is done over the volume of the pseudo-Brillouin zone, $(2\pi)^3 n_m = (4\pi/3)Q_M^3$. This gives $Q_M = 1.25$ Å^{-1} for water and $Q_M = 0.701$ Å^{-1} for sulfuric acid. Finally, the normalization constant K_g is determined from the experimental static structure factor of D_2SO_4 [30] and D_2O [44].

The two functions $g_1(\omega)$ and $g_2(\omega)$ represent the contribution of each mode to the density of states with their longitudinal weights $|\hat{\mathbf{Q}} \cdot \mathbf{e}_j^H|^2 = \cos^2\phi_j$, where $\mathbf{e}_j^H$ is the eigenvector of the jth mode at the hydrogen sites. A liquid is homogeneous and isotropic, therefore one longitudinal and two degenerate transverse modes are expected. The experimental $g(\omega)$ can be thus written as the sum of $g_1(\omega)$ and $g_2(\omega)$ weighted by $1/\cos^2\phi_j$, which accounts for the actual nature of the mode. The eigenvectors of the two modes must be orthogonal, therefore, if $\phi_1 \equiv \phi$ then $\phi_2 \equiv \pi/2 - \phi$ and the two transverse degenerated modes produce a single contribution with weight equal to $1/\sin^2\phi_j$. The weight angle ϕ can be obtained by comparing the experimental

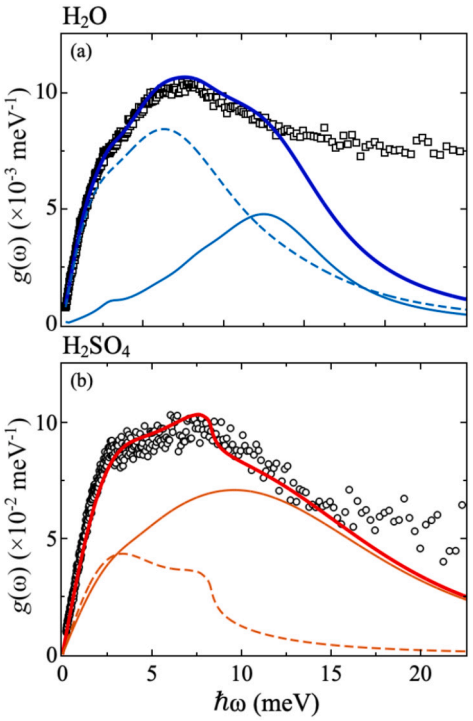

Fig. 3. Experimental density of states $g(\omega)$ projected onto the hydrogen sites for (a) H_2O (open black squares) and (b) H_2SO_4 (open black circles). The thick solid line is the fit with Eq. (5). The thin solid line and the dashed line show the behavior of the two components, $g_1(\omega)$ and $g_2(\omega)$ respectively, weighted as discussed in the text.

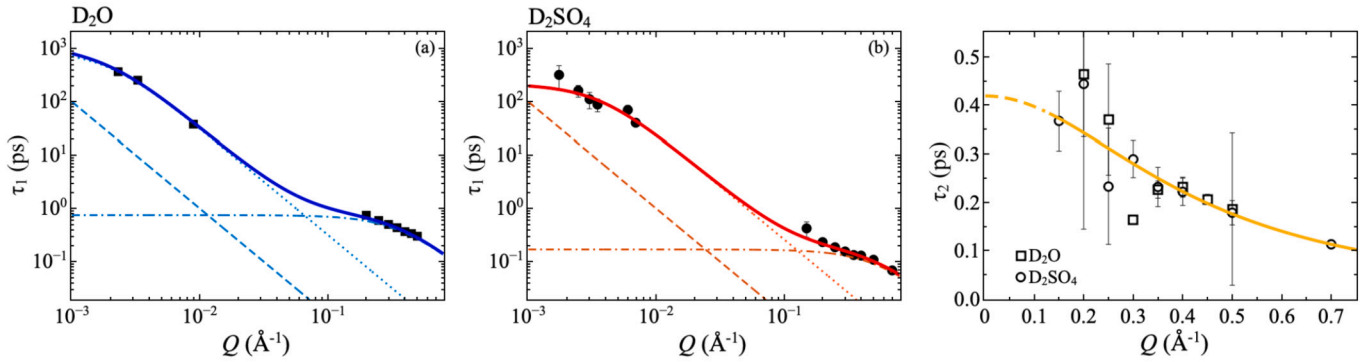

Fig. 4. Lifetime τ_1 of the mode $j = 1$ for (a) D_2O and (b) D_2SO_4. The thick solid line is the best fit to the data obtained with Eq. (6). The other lines represent the three components of Eq. (6): the viscosity one (dashed line) and the two Lorentzians (dotted and dash-dotted ones). (c) Comparison between the lifetime τ_2 of the $j = 2$ mode for D_2O (black open squares) and D_2SO_4 (black open circles). The solid yellow line is the best fit to the data obtained with a single Lorentzian function. The dashed part of the line is the hypothetical $Q \to 0$ behavior of τ_2.

$g(\omega)$ to the two components $g_1(\omega)$ and $g_2(\omega)$ through the fitting function:

$$g(\omega) = w_t \left[\frac{1}{\cos^2 \phi} g_1(\omega) + \frac{1}{\sin^2 \phi} g_2(\omega) \right], \tag{5}$$

where w_t is a measure of the projection on the H sites which depends on the molecular structure. The thick red line in Fig. 3 shows the excellent fit to the experimental data obtained with Eq. (5) in the range 0-15 meV, where the collective mode experiments provide an adequate information. For water the fit gives $\phi = 53° \pm 2°$, whereas for sulfuric acid $\phi = 28.4° \pm 0.3°$. This indicates that in sulfuric acid $j = 1$ has a mainly longitudinal character, whereas $j = 2$ has a mainly transverse character with an angle $\pi/2 - \phi = 61.6 \pm 0.3$ degs. Conversely, in water the longitudinal character is more uniformly distributed among two modes. In addition, the hydrogen-projected density of states in water is about three times higher, as expected, because the projection on the H atoms in the translational region should be roughly proportional to the inverse of the molecular mass.

The damping of the modes $\Gamma_j(Q)$ in Fig. 2(b) and (e) can be further analyzed by extracting its characteristic relaxation time $\tau_j(Q) = 2/\Gamma_j(Q)$. This quantity is shown in Fig. 4 for both D_2O and D_2SO_4. While $\tau_1(Q)$, the relaxation time for the $j = 1$ mode, is quite different in the two samples, see Fig. 4(a) and (b), τ_2 shows similar values suggesting a similar damping mechanism for $j = 2$.

To deepen our analysis of $\tau_1(Q)$, we can exploit available low-Q data obtained from light and ultraviolet Brillouin scattering [45]. For $Q \to 0$ only long-wavelength waves propagate and the attenuation can be written as $\Gamma(Q) = 2\eta Q^2$, where η is the kinematic viscosity [46]. Such a contribution is reported in Fig. 3(a) and (b) (dashed line) but it cannot account for the high-Q relaxation time. Data can be effectively modeled as a sum of three terms, the low-Q viscous attenuation plus two Lorentzian functions. The relaxation time $\tau_1(Q)$ turns out to be:

$$\begin{aligned} \tau_1(Q) &= \frac{1}{\eta Q^2} + \tau_\alpha + \tau_\beta \\ &= \frac{1}{\eta Q^2} + \frac{C_\alpha}{Q_\alpha^2 + Q^2} + \frac{C_\beta}{Q_\beta^2 + Q^2}, \end{aligned} \tag{6}$$

where C_i are amplitudes and Q_i critical wavevectors of the ith process with $i = \alpha, \beta$. This simple model shows a remarkable good agreement with data, solid lines in Fig. 4. The damping process was described by a Lorentian function since it has a finite 3D Fourier transform $\tau_i(r)$, so we can determine the mean square radius of the ith damping processes $\langle r_i^2 \rangle$ as:

$$\langle r_i^2 \rangle = \frac{\int_0^\infty \tau_i(r) r^2 dr}{\int_0^\infty \tau_i(r) r^4 dr} = \frac{6}{Q_i^2}. \tag{7}$$

The $Q \to 0$ viscous relaxation and the $i = \alpha$ Lorentzian damping process have macroscopic character with a root mean square radius of about one micrometer. Conversely, the $i = \beta$ process is on the molecular scale, and the root mean square radius is equal to 6.5 ± 0.2 Å for water and 4.55 ± 0.09 Å for sulfuric acid.

If we consider $\tau_2(Q)$, we cannot extend data to $Q \to 0$ since the transverse mode disappears in the macroscopic limit. In the explored Q-range, we can try to model the data with a single Lorentzian function. This limited fit provides a critical value $Q_c = 0.6 \pm 0.1$ Å^{-1} that gives a root mean square radius of 4.0 ± 0.2 Å. Moreover, the amplitude of the Lorentzian function provides an hint on the macroscopic lifetime value of the $j = 2$ mode. This turns out to be 0.42 ± 0.01 ps, which is compatible with the H-bond lifetime, as obtained by numerical simulations in water and sulfuric acid-water mixtures [47,48]. This justifies the similar damping in the two systems.

4. Conclusions

We studied the collective dynamics of two hydrogen bonded liquids: water and sulfuric acid. These two systems share a similar hydrogen bond network although their chemical nature is very different. We found that their collective dynamics is mainly made up of two interacting modes. The highest energy excitation is the prolongation of the longitudinal acoustic mode and presents a strong fast sound, with a remarkably high ratio c_∞/c_0 equals to 2.73 ± 0.06 for water and 2.62 ± 0.02 for sulfuric acid. The low-lying modes have an average energy of about 7.0 ± 0.3 meV and 4.7 ± 0.8 meV and display a smooth Q dependence. The transition between c_0 and c_∞ is well described within a mode-interaction model. Following a crystal-like approach, the comparison between the total $g(\omega)$ and the single-mode density of states allows to identify the relative transverse nature of the low-lying mode in a direct way. In particular, $j = 2$ shows a major transverse nature in D_2SO_4, where polarization effects appear to be stronger.

In liquid Zn [6] and methanol [11], the existence of such a transverse mode was related to the presence of anisotropic interactions. In hydrogen-bonded liquids, these might be ascribed to the directional character of the hydrogen bond network, making the observed complex dynamics a general distinctive characteristic of such class of liquids. Of course, when the probed length scale is increased, i.e. Q is decreased towards the hydrodynamic region, the microscopic structure becomes irrelevant and the low-lying mode eventually vanishes, creating a gap in the dispersion relation [38]. It is worth noting that the lifetime of the $j = 2$ modes is almost identical in the two liquids. The similar $\tau_2(Q)$ behavior suggests a similar damping mechanism and thus a similar origin for the transverse mode. The similarity between $\tau_2(0)$ and the lifetime of hydrogen bonds in water and sulfuric acid supports the origin of the $j = 2$ mode as the result of anisotropic interactions.

A still open question concerns the optic or acoustic nature of the low energy mode. Molecular dynamics simulations in water suggest that the transverse mode has an acoustic nature [49]. However, neither simulations nor experiments can access the very low-Q region and, in both acoustic and optic cases, the structure factor of the mode is expected to vanish. In addition, in the very low-Q region, a transverse acoustic mode should be overdamped and no really acoustic-like behavior can be present [50,38]. Therefore this question seems ill defined and deserves further consideration.

It is worth noting that the proposed method to determine the longitudinal or transverse nature of collective modes can be easily applied to any system that allows the determination of the density of states. Moreover, the planned development of INS instrumentation with polarization analysis will allow to measure both $S(Q,\omega)$ and $S_{\mathrm{self}}(Q,\omega)$ in a single experiment in many materials, thus opening the way to a vast area of new investigations [7,51].

CRediT authorship contribution statement

M. Zanatta: Methodology, Writing – review & editing. **A. Orecchini:** Investigation, Writing – review & editing. **F. Sacchetti:** Conceptualization, Methodology, Writing – review & editing. **C. Petrillo:** Writing – review & editing.

Declaration of competing interest

The authors declare that they have no known competing financial interests or personal relationships that could have appeared to influence the work reported in this paper.

Data availability

Data will be made available on request.

Acknowledgements

The Institut Laue Langevin (Grenoble, France) is gratefully acknowledged for allocation of beamtime at IN1 and IN5 spectrometers. This work has been funded by the European Union - NextGenerationEU under the Italian Ministry of University and Research (MUR) National Innovation Ecosystem grant ECS00000041 - VITALITY - CUP J97G22000170005.

References

[1] L.D. Landau, E.M. Lifshitz, Statistical Physics, Pergamon, Oxford, 1969.
[2] F. Sette, et al., Transition from normal to fast sound in liquid water, Phys. Rev. Lett. 77 (1996) 83.
[3] C. Petrillo, F. Sacchetti, B. Dorner, J.-B. Suck, High-resolution neutron scattering measurement of the dynamic structure factor of heavy water, Phys. Rev. E 62 (2000) 3611.
[4] F. Sacchetti, J.-B. Suck, C. Petrillo, B. Dorner, Brillouin neutron scattering in heavy water: evidence for two-mode collective dynamics, Phys. Rev. E 69 (2004) 061203.
[5] E. Pontecorvo, et al., High-frequency longitudinal and transverse dynamics in water, Phys. Rev. E 71 (2005) 011501.
[6] M. Zanatta, et al., Collective ion dynamics in liquid zinc: evidence for complex dynamics in a non-free-electron liquid metal, Phys. Rev. Lett. 114 (2015) 187801.
[7] C. Petrillo, F. Sacchetti, Future applications of the high-flux thermal neutron spectroscopy: the ever-green case of collective excitations in liquid metals, Adv. Phys. X 6 (2021) 1871862.
[8] T.W. Martin, Z.S. Derewenda, The name is bond—H bond, Nat. Struct. Biol. 6 (1999) 403–406.
[9] K. Amann-Winkel, et al., X-ray and neutron scattering of water, Chem. Rev. 116 (2016) 7570.
[10] G. Garberoglio, F. Pasqualini, G. Sutmann, R. Vallauri, Dynamical properties of hydrogen bonded liquids, J. Mol. Liq. 96–97 (2002) 19–29.
[11] S. Bellissima, et al., Switching off hydrogen-bond-driven excitation modes in liquid methanol, Sci. Rep. 7 (2017) 10057.
[12] J. Teixeira, M.-C. Bellissent-Funel, S.H. Chen, B. Dorner, Observation of new short-wavelength collective excitations in heavy water by coherent inelastic neutron scattering, Phys. Rev. Lett. 54 (1985) 2681.
[13] G. Ruocco, et al., Equivalence of the sound velocity in water and ice at mesoscopic wavelengths, Nature 379 (1996) 521.
[14] A. Rahman, F.H. Stillinger, Propagation of sound in water. A molecular-dynamics study, Phys. Rev. A 10 (1974) 368–378.
[15] G. Ruocco, F. Sette, The high-frequency dynamics of liquid water, J. Phys. Condens. Matter 11 (1999) R259.
[16] D. Ishikawa, A.Q.R. Baron, J. Phys. Soc. Jpn. 90 (2021) 083602.
[17] R. Angelini, et al., Structural and microscopic relaxation processes in liquid hydrogen fluoride, Phys. Rev. Lett. 88 (2002) 255503.
[18] F. Sette, et al., Determination of the short-wavelength propagation threshold in the collective excitations of liquid ammonia, Phys. Rev. Lett. 84 (2000) 4136.
[19] P. Giura, R. Angelini, F. Datchi, G. Ruocco, F. Sette, High frequency dynamics and structural relaxation process in liquid ammonia, J. Chem. Phys. 127 (2007) 084508.
[20] A. Orecchini, A. Paciaroni, A. De Francesco, C. Petrillo, F. Sacchetti, Collective dynamics of protein hydration water by Brillouin neutron spectroscopy, J. Am. Chem. Soc. 131 (2009) 4554.
[21] A. Paciaroni, et al., Vibrational collective dynamics of dry proteins in the terahertz region, J. Phys. Chem. B 116 (2012) 3861–3865.
[22] E. Cornicchi, et al., Collective density fluctuations of DNA hydration water in the time-window below 1 ps, J. Chem. Phys. 135 (2011) 025101.
[23] F. Sebastiani, et al., Collective THz dynamics in living Escherichia coli cells, Chem. Phys. 424 (2013) 84–88.
[24] M. Longo, et al., Terahertz dynamics in human cells and their chromatin, J. Phys. Chem. Lett. 5 (2014) 2177.
[25] A.G.G.M. Tielens, The molecular universe, Rev. Mod. Phys. 85 (2013) 1021.
[26] A.D. Fortes, M. Choukroun, Phase behaviour of ices and hydrates, Space Sci. Rev. 153 (2010) 185–218.
[27] E. Marcq, J.-L. Bertaux, F. Montmessin, D. Belyaev, Variations of sulphur dioxide at the cloud top of Venus's dynamic atmosphere, Nat. Geosci. 6 (2013) 25–28.
[28] J. Almeida, et al., Molecular understanding of sulphuric acid–amine particle nucleation in the atmosphere, Nature 502 (2013) 359.
[29] A.R. Moodenbaugh, et al., Neutron-diffraction study of polycrystalline H_2SO_4 and H_2SeO_4, Phys. Rev. B 28 (1983) 3501.
[30] C. Andreani, C. Petrillo, F. Sacchetti, The structure of liquid sulphuric acid, Mol. Phys. 58 (1986) 299.
[31] Y. Kameda, et al., Hydrogen-bonded structure in aqueous sulfuric acid solutions, J. Mol. Liq. 65 (1995) 305.
[32] S.W. Lovesey, Theory of Neutron Scattering from Condensed Matter, vol. 1, Oxford University Press, Oxford, 1986.
[33] C. Petrillo, F. Sacchetti, Analysis of neutron diffraction data in the case of high-scattering cells. II. Complex cylindrical cells, Acta Crystallogr., Sect. A 48 (1992) 508.
[34] M. Zanatta, A. Fontana, A. Orecchini, C. Petrillo, F. Sacchetti, Inelastic neutron scattering investigation in glassy $SiSe_2$: complex dynamics at the atomic scale, J. Phys. Chem. Lett. 4 (2013) 1143.
[35] M. Inui, et al., Peculiar atomic dynamics in liquid GeTe with asymmetrical bonding: observation by inelastic X-ray scattering, Phys. Rev. B 97 (2018) 174203.
[36] N.P. Kryuchkov, V.V. Brazhkin, S.O. Yurchenko, Anticrossing of longitudinal and transverse modes in simple fluids, J. Phys. Chem. Lett. 10 (2019) 4470–4475.
[37] G. D'Angelo, et al., Multiple interacting collective modes and phonon gap in phospholipid membranes, J. Phys. Chem. Lett. 9 (2018) 4367–4372.
[38] R.M. Khusnutdinoff, et al., Collective modes and gapped momentum states in liquid Ga: experiment, theory, and simulation, Phys. Rev. B 101 (2020) 214312.
[39] L.E. Bove, C. Petrillo, F. Sacchetti, Ion density fluctuations in liquid metals: the strongly interacting ion-electron plasma, Condens. Matter Phys. 11 (2008) 119.
[40] L. Sani, C. Petrillo, F. Sacchetti, Determination of the interstitial electron density in liquid metals: basic quantity to calculate the ion collective-mode velocity and related properties, Phys. Rev. B 90 (2014) 024207.
[41] G. Monaco, V.M. Giordano, Breakdown of the Debye approximation for the acoustic modes with nanometric wavelengths in glasses, Proc. Natl. Acad. Sci. USA 106 (2009) 3659.
[42] N. Violini, A. Orecchini, A. Paciaroni, C. Petrillo, F. Sacchetti, Phys. Rev. B 85 (2012) 134204, and Refs. therein.
[43] L. Orsingher, et al., High-frequency dynamics of vitreous $GeSe_2$, Phys. Rev. B 82 (2010) 115201, and Refs. therein.
[44] M.-C. Bellissent-Funel, Recent structural studies of liquid D_2O by neutron diffraction, in: J.C. Dore, J. Teixeira (Eds.), Hydrogen Bonded Liquid, Springer, 1991, pp. 117–128.
[45] P. Benassi, M. Nardone, A. Giugni, Sound dispersion and attenuation in concentrated H_2SO_4 by visible and ultraviolet Brillouin spectroscopy, J. Chem. Phys. 135 (2011) 034503.
[46] F.H. Rhodes, C.B. Barbour, The viscosities of mixtures of sulfuric acid and water, Ind. Eng. Chem. 5 (1923) 850.
[47] M. Canales, E. Guàrdia, A comparative molecular dynamics study of sulfuric and methanesulfonic acids, J. Mol. Liq. 224 (2016) 1064–1073.
[48] M. Canales, E. Guàrdia, Computer simulation study of ion-water and water-water hydrogen bonds in sulfuric acid solutions at low temperatures, J. Mol. Liq. 347 (2022) 118351.

[49] M. Sampoli, G. Ruocco, F. Sette, Mixing of longitudinal and transverse dynamics in liquid water, Phys. Rev. Lett. 79 (1997) 1678.
[50] K. Trachenko, V.V. Brazhkin, Collective modes and thermodynamics of the liquid state, Rep. Prog. Phys. 79 (2016) 016502.
[51] A. Arbe, et al., Coherent structural relaxation of water from meso-to intermolecular scales measured using neutron spectroscopy with polarization analysis, Phys. Rev. Res. 2 (2020) 022015(R).